



In-Orbit Commissioning of Czech Nanosatellite VZLUSAT-1 for the QB50 Mission with a Demonstrator of a Miniaturised Lobster-Eye X-Ray Telescope and Radiation Shielding Composite Materials

V. Daniel¹ · A. Inneman² · I. Vertat³ · T. Baca² · O. Nentvich² · M. Urban² · V. Stehlíkova² · L. Sieger² · P. Skala² · R. Filgas⁴ · V. Zadrazil¹ · R. Linhart³ · J. Masopust³ · T. Jamroz¹ · L. Pina⁵ · V. Marsíková^{2,6} · L. Mikulicková^{7,8} · E. Belas⁹ · S. Pospisil⁴ · Z. Vykydal^{4,10} · Y. Mora⁴ · R. Pavlica¹¹

Received: 6 June 2018 / Accepted: 6 February 2019 / Published online: 1 July 2019
© Springer Nature B.V. 2019

Abstract This paper presents the results of in-orbit commissioning of the first Czech technological CubeSat satellite of VZLUSAT-1. The 2U nanosatellite was designed and built during the 2013 to 2016 period. It was successfully launched into Low Earth Orbit of 505 km altitude on June 23, 2017 as part of international mission QB50 onboard a PSLV C38 launch

Multi-Point Measurements of the Thermosphere with the QB50 Mission
Edited by David Miles, Robert Wicks and James Burch

✉ V. Daniel
daniel@vzlu.cz

I. Vertat
ivertat@kae.zcu.cz

T. Baca
tomas.baca@fel.cvut.cz

O. Nentvich
ondrej.nentvich@fel.cvut.cz

M. Urban
martin-urban@fel.cvut.cz

V. Stehlíkova
veronika.stehlikova@fel.cvut.cz

L. Sieger
sieger@fel.cvut.cz

P. Skala
skalape4@fel.cvut.cz

R. Filgas
robert.filgas@utef.cvut.cz

R. Linhart
rlinhart@kae.zcu.cz

J. Masopust
masopust@kae.zcu.cz

vehicle. The satellite was developed in the Czech Republic by the Czech Aerospace Research Centre, in cooperation with Czech industrial partners and universities. The nanosatellite has three main payloads. The housing is made of a composite material which serves as a structural and radiation shielding material. A novel miniaturized X-Ray telescope with lobster-eye optics and an embedded Timepix detector represents the CubeSat's scientific payload. The telescope has a wide field of view. VZLUSAT-1 also carries the FIPEX scientific instrument as part of the QB50 mission for measuring the molecular and atomic oxygen concentration in the upper atmosphere.

Keywords CubeSat · QB50 · Space radiation · Pixel detector Timepix · Carbon composite · Lobster-Eye optics

1 Introduction

VZLUSAT-1 was built as a Czech technological nanosatellite to demonstrate newly developed materials and approaches potentially usable for future space missions. The development team established in 2013 was created as a cooperative group, with members from research centers, universities and commercial companies from the Czech Republic. The nanosatellite was selected to participate in international project QB50, which aimed to create a network of small satellites in the lower thermosphere to measure properties of this not very well studied atmospheric layer. All participating satellites were required to carry one prescribed scientific instrument on board, while the remaining accommodation was available for use by the teams.

L. Pina
ladislav.pina@fjfi.cvut.cz

V. Marsikova
Veronika.Marsikova@rigaku.com

L. Mikulickova
mikulickova@tts-co.eu

R. Pavlica
richard.pavlica@5m.cz

¹ Czech Aerospace Research Centre, Prague, Czech Republic

² Faculty of Electrical Engineering, Czech Technical University in Prague, Prague, Czech Republic

³ University of West Bohemia in Pilsen, Pilsen, Czech Republic

⁴ Institute of Experimental and Applied Physics, Czech Technical University in Prague, Prague, Czech Republic

⁵ Faculty of Nuclear Sciences and Physical Engineering, Czech Technical University in Prague, Prague, Czech Republic

⁶ Rigaku Innovative Technologies Europe s.r.o., Prague, Czech Republic

⁷ University of Chemistry and Technology Prague, Prague, Czech Republic

⁸ TTS, s.r.o., Prague, Czech Republic

⁹ Charles University, Prague, Czech Republic

¹⁰ Present address: Czech Metrology Institute, Prague, Czech Republic

¹¹ 5M, s.r.o., Kunovice, Czech Republic

One experiment serves for testing the carbon fiber material with improved radiation shielding properties. Three different properties are measured: the ageing of the mechanical properties of the composite, the radiation shielding properties and the evaporation of water and other residuals from the composite. The mechanical properties of the radiation-hardened carbon composite are evaluated as a function of the measured characteristic Young's modulus of elasticity, which can be deduced by a Health monitoring (HM) panel from changes in the eigenfrequencies of the beam. The measurements of the radiation shielding properties are realized by three XRB (X-Ray Background) PIN diodes with different shielding and a CdTe detector with data that are processed by a complex programmable logic device (CPLD) on-board. The last measured property is focused on the evaporation of water and other residuals from the carbon composite. Three different types of sensors, two of which are organic and one of which is inorganic, are used for measurements of volatiles. Material verification is described in more detail in Daniel et al. (2016), Urban et al. (2017).

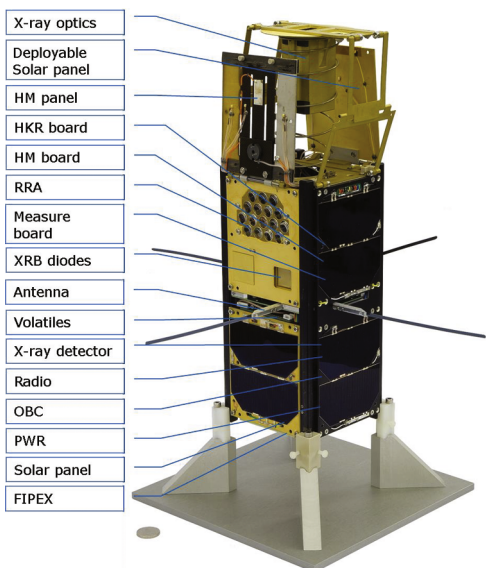
The second payload is an experimental telescope based on an X-Ray optical system (Pína et al. 2015) with a Timepix pixel detector (Llopert et al. 2007; Baca et al. 2016) as focal plane imager. This telescope uses a one-dimensional (1D) lobster-eye (LE) optics (Pína et al. 2016; Angel 1979; Schmidt 1975). This provides a relatively wide field of view and a reasonable range of focusing energies up to 15 keV. These parameters make it promising for all-sky monitoring (Hudec 2017), for Sun monitoring and for monitoring Terrestrial Gamma-Ray Flashes (TGF) (Dániel et al. 2016). Timepix is a single-photon-counting detector based on a highly integrated ASIC (Application Specific Integrated Circuit) chip. The detector is able to work in three different modes: particle counter, energy measurement and measurement of the particle interaction time. This kind of detector, developed at CERN within the Medipix2 collaboration (Llopert et al. 2007), was deployed successfully in orbit (Turecek et al. 2011) and in on the Proba-V mission (Granja et al. 2016), in addition to its intended use for measurements during a rocket experiment (Dániel et al. 2017; Stehlikova et al. 2017). A combination of the Timepix detector and LE optics is unique and has never been launched to space environment. The detector is sensitive to X-Rays in the range of 3–25 keV (near 100% efficiency) and up to 60 keV (decreasing efficiency) with the upper range given by the detection efficiency of the equipped silicon sensor (Urban et al. 2017).

The third experiment onboard the satellite, provided by the QB50 project, is the FIPEX instrument for detecting residual atomic and molecular oxygen. The payload is alive and responding, but is not fully operational. A few seconds after it was powered on, FIPEX terminated the measurements prematurely for unknown reasons. This may have been caused by FIPEX's power issues, which were described by QB50 commissioning as functional non-conformance—very high sensitivity on the 3.3 V line. Another explanation may be an incorrect FIPEX script interpretation by the Onboard computer (OBC). Efforts to revive FIPEX SU are still ongoing.

2 Spacecraft Overview

The satellite consists of two 1 U units, which have unified parameters with overall dimensions of 100 mm × 100 mm × 230 mm (folded) and 100 mm × 100 mm × 340 mm after deployment. As shown in Fig. 1, the deployable segment with the lobster-eye collimator is placed on top. When folded out, the optical path, going through the middle of the body of the body, is 25 cm long, and ejection, as well as the keeping of the position of the collimator, is provided by a spring. There are also two deployable panels: the HM panel formed from the examined carbon fiber material, and a solar panel. An array of 16 reflectors is placed under

Fig. 1 Description of the VZLUSAT-1 nanosatellite (Urban et al. 2017). A photo of the engineering model is displayed



the HM panel. These are intended to help to determine the exact position of the satellite using laser pulses from Earth. There is a Measure board with two functions in the bottom part of the satellite. The first function, which will be switched on most of time in orbit, records the temperature values from 27 thermometers (PT1000) placed in all significant places on the satellite. The second function of the Measure board is to collect and process data from the radiation shielding monitor.

The four rod antennas, which are folded inside during integration and launch, have been located between the two 1 U units. Under this board, there is a payload with volatile sensors, which are inside the body (2 items) and outside the body (1 item) of the satellite. One double magnet-torque coil, for use as a stabilization system, has also been placed on this board.

The bottom end of the X-Ray telescope focuses the optical path onto the focal plane with the Timepix detector and its electronics board. Beneath are located the radio board (GOMspace NanoCom U482C), which enables communication with the Pilsen ground station, the on-board computer (GOMspace OBC, NanoMind A712D), which manages the general functionality and timing of the satellite, the board with the power supply (GOMspace NanoPower P31u with two lithium-ion batteries) for individual payloads, and a rechargeable battery pack. The last part of the satellite is the FIPEX experiment, which has to be in the direction of flight for proper functionality and effectiveness of the measurements. A more detailed description of the satellite, its parts, its operation and its mission is given in Urban et al. (2017).

3 Spacecraft Commissioning

VZLUSAT-1 was successfully launched on 23rd June 2017 as a part of international mission QB50 onboard the Indian PSLV C38 rocket. As VZLUSAT-1 was released off the rocket launcher, the commissioning mode was applied for the first 30 minutes (in accordance the CalPoly CubeSat standards req. 2.4.2). Antennas, one solar panel and the Health monitoring

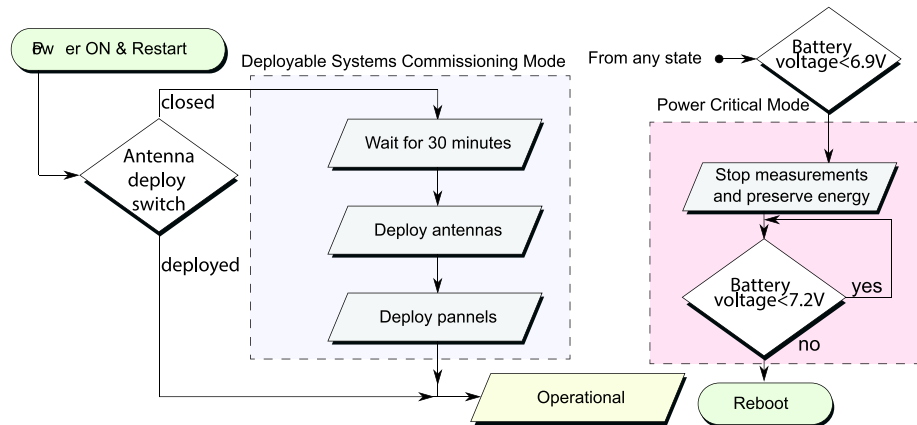


Fig. 2 A diagram of the OBC Master task, a routine responsible for boot sequence of the main computer. The task is responsible for antennas deployment during the commissioning mode and for a failsafe mode in a case of low battery voltage

panel were successfully deployed just after the first booting up of the satellite. The lobster-eye optics was released after three months.

The battery voltage is continuously monitored by the OBC Master task (Fig. 2) to prevent a drop below the critical level of 6.9 V ($\sim 10\%$ battery capacity). The power critical mode has never in fact been entered in orbit.

The OBC itself showed stable operation during the first three months. However, VZLUSAT-1 faces recurring OBC restarts in periods from 90 to 270 minutes. Restarts occur during violent temperature changes on the satellite. It is considered that a payload is temporarily blocking the main on-board communication bus (shared I²C), which causes the OBC to reset. Because of the multimaster scheme, the bus remains blocked. The watchdog of the Power board then resets the OBC after not being switched on for 10 minutes or more. Payloads which are directly connected to the OBC are not affected by this procedure. Payloads connected through the main I²C bus are out of order during this 10 minute period.

It was shown that after the restart, the OBC failed to continue measuring according to the Planner script when data storage filled more than 50%. To prevent interruption, measurements have to be carefully scheduled and data generating/downloading need to be kept balanced.

So far, several SEE (Single Event Effects) have occurred and have caused chunk numbering to be reset in the flash storage or configuration deleting from payloads. In addition, harder SEEs were registered, causing Flash storage to exhibit errors. The UFFS file system places affected storage blocks out of order. VZLUSAT-1 detects approx. four SEEs per month. Most commonly, this takes place in regions of the Van Allen radiation belts especially the South Atlantic Anomaly.

3.1 Attitude Determination and Control System

The Attitude Determination and Control System (ADCS) of the VZLUSAT-1 satellite comprises three magnetorquer coils oriented mutually perpendicularly, working as actuators. The HMC5843 single chip vector magnetometer is utilized as the only sensor input of the system. The coils are driven by the internal hardware drivers of the GomSpace NanoMind

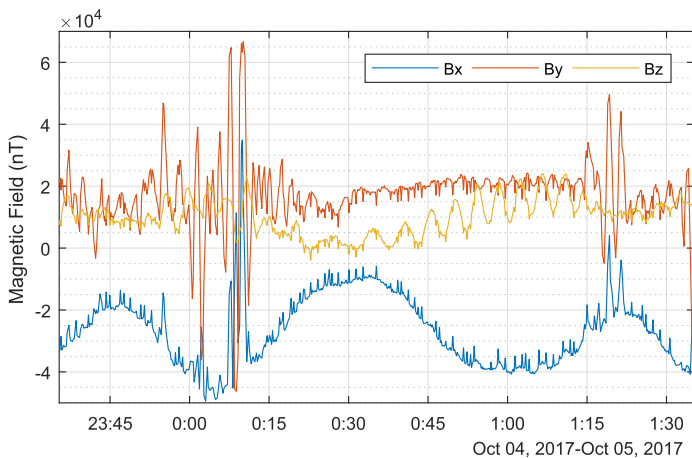


Fig. 3 Magnetic induction flux density x, y, z components of satellite Reference Frame vs. time represented by the lower-blue curve, the upper-red curve and the middle-yellow curve, respectively

A712D On-board Computer system. The first magnetometer data planned to be used for the ADCS were corrupted by noise and cyclic swing of the signal probably from platform operations. A deeper examination showed that the cyclic swing is caused by the beacon and radio communication as shown in Fig. 3.

During the commissioning phase it became apparent that the satellite as a whole represents a permanent magnetic dipole. The magnetic moment is 2.65 times higher than the maximum magnetic moment 0.0817 A m of a single magnetorquer, rendering the ADCS actuators powerless. No matter how limited the ability of the actuators is, attempts are still made to control the attitude of the satellite. The permanent magnetic dipole of the satellite is likely to be the superposition of magnetic dipoles of some components of the internal electronics, e.g., chokes with ferrite cores especially those with an open magnetic circuit, and the magnetic dipoles of some structural mechanical components that are ferromagnetic with significant magnetic remnants, such as screws, washers, nuts, springs and the radio antennas poles aboard the satellite. These ferromagnetic components became magnetized unwittingly as a by-effect of the vibration testing that the satellite was subjected to, due to the strong magnetic actuator, the whose strong magnetic field of which inevitably reached the tested sample. This was detected during the testing campaign. The satellite was later demagnetized to order lower then 1 times the single magnetorquer maximum magnetic moment to ensure control capability. However, the satellite became magnetized again between the delivery of to the satellite to the launch service company and the in-orbit phase. We had no control during this phase and we are therefore not able to estimate the reason for the magnetization. However, the lessons that have been learned from this incident will be very important for future missions.

Because of the present apparently permanent magnetic dipole of a satellite of this great magnitude, the satellite is stabilized orientation-wise along the magnetic field of the Earth. In additionally, small oscillations of up to approximately 10 degrees peak-to-peak amplitude are observed in the downloaded telemetry data readouts from the vector magnetometer instrument.

The magnetometric data have been processed aboard the satellite, producing raw estimates of unit quaternions representing the current attitude of the satellite. These raw data

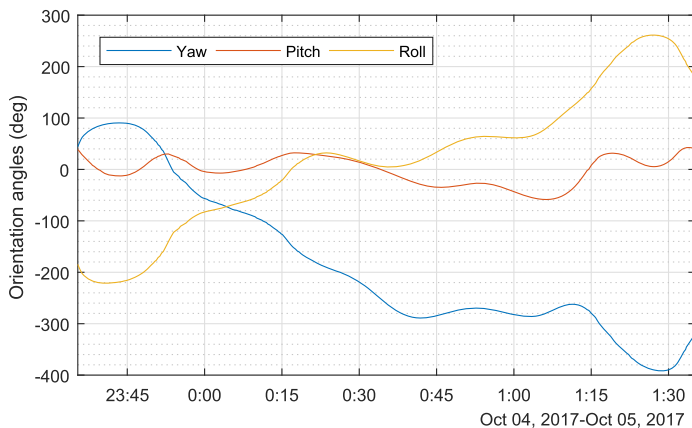


Fig. 4 Yaw, Pitch, and Roll angles representing the attitude of the satellite

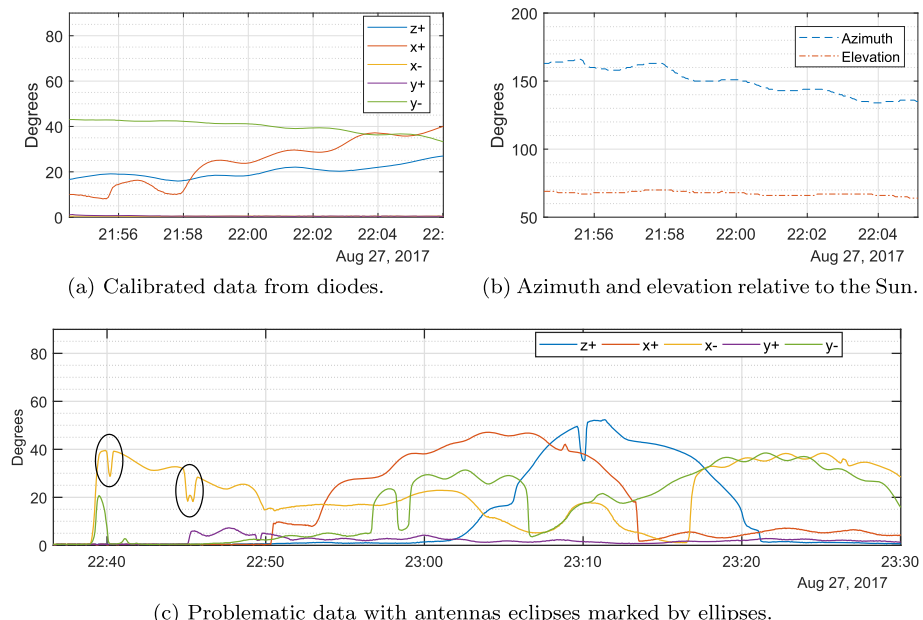


Fig. 5 Data from photodiodes and result of attitude calculation

have been further processed on the ground to produce filtered estimates of these quantities. See Fig. 4 for a sample data set of these filtered unit quaternions, transformed into yaw, pitch and roll intrinsic rotation angles representing the satellite attitude.

The magnetometric ADCS is backed by five SILONEX SLCD-61N8 photodiodes positioned on all sides except the side where the FIPEX instrument is located. After calibration, the voltage can be directly converted to angles (Fig. 5a), and the attitude to the Sun can be estimated (Fig. 5b). Data from the diodes can be combined with NORAD TLE, allowing the position and attitude to be calculated. The data are occasionally corrupted due to shad-

ows cast by satellite antennas or solar panels (before x-ray optics are deployed) and need additional data analysis to filter these moments (Fig. 5c).

3.2 Miniaturised X-Ray Telescope

The miniaturized X-Ray telescope consists of two separate components—the multi-foil 1D X-Ray “lobster-eye” optics (Pína et al. 2016) and the sensor board equipped with a Timepix detector (Baca et al. 2016) on the focal plane of the telescope. The use of optics to focus X-Rays on a detector is a viable solution in cases where the intensity of the impinging X-Ray radiation falls below the sensitivity of the detector, e.g., while monitoring astrophysical objects in space, or phenomena in the Earth’s atmosphere.

The detector part of the telescope serves two purposes on board VZLUSAT-1. First, as a focal plane imager for the X-Ray telescope, and second, as a dosimetry module and a radiation monitor. Both functions are carried out by the Timepix (Llopert et al. 2007), a hybrid semiconductor ASIC chip detector with resolution 256×256 pixels. Each one of the 65 536 pixels of the detector can be individual configured to eliminate thermal noise before digitization of the signal. All pixels can be equalized to produce images clean of any pixel noise regardless of the acquisition time. Thanks to the equalization, any signal obtained by the detector is considered to be a direct effect of an ionizing radiation. The detector is attached to a silicon sensor ($14 \text{ mm} \times 14 \text{ mm} \times 0.3 \text{ mm}$) that is capable of sensing various ionizing particles, such as photons (X-Rays in the range of 3–60 keV) and charged particles including electrons, protons and ions. Each detected particle leaves a single trace in the image, by which it can be classified and evaluated. The sensor is mounted on a compact *USB Lite interface* (Vykydal and Jakubek 2011), which was modified for the constraints of the low-powered and computationally limited hardware of the CubeSat satellite. Particular focus was given to onboard processing of measured data to maximize the information yield from data downloaded to the ground via the limited downlink. Detailed description of modes of operation and methods of processing can be found in Baca et al. (2016). The sensor board was successfully brought to life by the ground segment during a fully-teleoperated contact. Initial debugging data confirmed the operational capability of the payload processor. Both the Timepix sensor and the onboard FRAM memory responded positively. Subsequently, the first image acquisition was conducted, producing an 8×8 -pixel compressed image, which confirmed the correct operation of the detector. Furthermore, full-resolution acquisitions were conducted to estimate the energy threshold, which is a vital step towards capturing images free of any noise. See Fig. 6 for examples of the first orbital images captured by the Timepix sensor.

Timepix produced the first image in orbit on July 13, 2017, and has since provided more than 26000 orbital measurements. Most of the data were processed onboard to produce energy histograms and low-resolution binned images. Periodically repeated measurements can be conducted using the scripting functionality of the satellite main computer. Dosimetry measurements can be collected over a period of a single day and can be further processed to obtain estimates of the radiation in the whole low-Earth orbit. See Fig. 7 for an example of a dosimetry map, reconstructed from a single day of sampling.

The optical part of the X-Ray telescope is a 1D lobster-eye collimator. Besides being capable of collimating a beam of X-Ray photons, the instrument was designed to reflect the otherwise blocked light on the focal plane. The increased gain of the signal is necessary for identifying faint sources and for being able to distinguish them from the background radiation. The optics module consists of 56 pieces of $145 \mu\text{m}$ thick, flat, glass foils. The foils are separated by $300 \mu\text{m}$ gaps. Surface of the foils is gold-coated on both sides, which

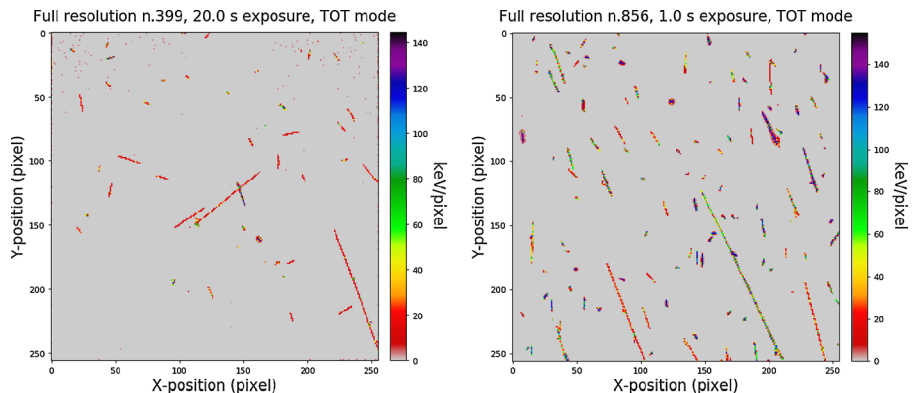


Fig. 6 Detection and visualization of space radiation by the Timepix detector in the VZLUSAT-1 satellite. (a) The image was produced during threshold level identification in the early stages of commissioning. Note the higher amount of single-pixel events (noise) near the upper edge of the image. Additional, tracks of ionizing particles are present in the image. (b) The first full-resolution image taken in the middle of the South-Atlantic Anomaly. Each isolated mark (track) in the image corresponds to an effect of a single ionizing particle. The total value of pixels in a track corresponds to an energy dissipated by a particle in the sensor

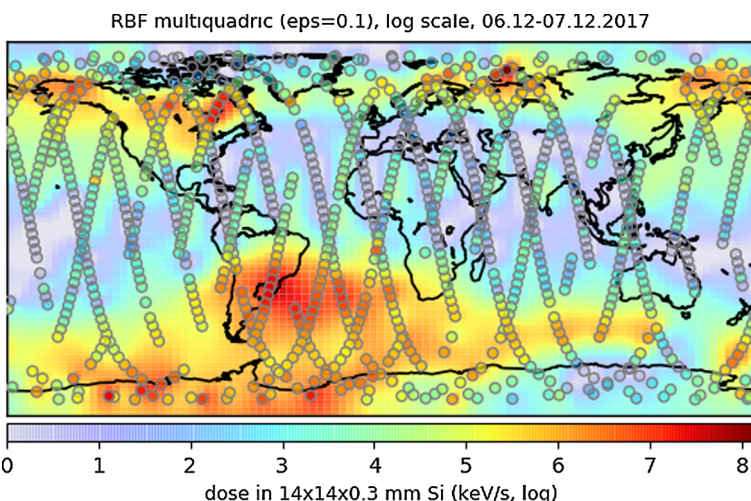


Fig. 7 Dosimetry map of radiation captured on December 6th, 2017. The logarithmic scale shows the amount of radiation deposited in the $300\ \mu\text{m}$ silicon sensor of the Timepix detector. The circled points show the points of measurement. The map was interpolated using multiquadric RBF with $\varepsilon = 0.1$

allows reflections of incoming X-Ray photons onto the Timepix sensor. Photons can be reflected when coming at incident angles under 0.5° from the telescope optical axis. The glass foils are arranged in such a way that, with a focal length of 250 mm, the telescope can detect sources within a 3° field of view (FOV). The X-Ray optics resides on a deployable platform, which is folded to conceal the optics during launch. Additionally, a Tungsten bar is installed in front of the optics aperture to serve as a coded mask. Thus the position of a single point source can be identified by extracting the position of a 1D focus and a shadow pattern, which are both created on the focal plane See Fig. 8a for an example of the expected

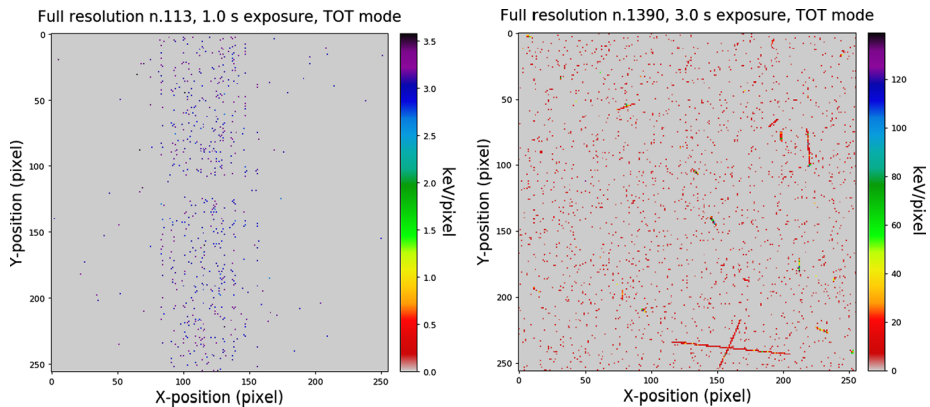


Fig. 8 The expected image of a point source in the FOV of the telescope (a) was captured during the full-function tests before the launch. The actual image of solar X-Rays (b) is blurred due to the uncontrolled motion of the satellite

output of the telescope. A detailed description of the telescope payload can be found in Baca et al. (2016).

Prior to the deployment of the optics, the automatic UV trigger mechanism was tested, with the goal to show the collimating properties of the retracted optics. Even with the optics retracted, a position of the X-Ray source in the FOV can be theoretically obtained. However, due to the unstabilized rotational motion of the satellite, exposure times of the celestial objects are limited to only hundredths of a second, before the object leaves the FOV. Figure 8 shows the expected and obtained images captured using the automated UV trigger mechanisms. The optics was deployed on October 4th, 2017, 104 days into the mission. Future measurements of the telescope payload will be focused on short exposures of the solar disc with the goal to identify the weak signal in the surrounding background ionizing radiation, even when the satellite is undergoing tumbling.

3.3 Ageing Properties of the Composite

The mechanical properties of radiation-hardened carbon composite are evaluated as a function of the measuring characteristic Young's modulus of elasticity, which represents the stiffness of the material and carries information about the degradation of the carbon composite structure in time (Hana et al. 2015). The modulus is influenced by radiation, vacuum, periodical temperature changes from -50°C to $+80^{\circ}\text{C}$, with a period of 94 minutes and also by the orbital conditions. The orbit of VZLUSAT-1, at 505 km altitude, provides the possibility of several years of testing, so the resulting data can show relevant trends in material ageing.

The payload for measurements of the mechanical properties has two parts. The first part is the health monitoring panel (Fig. 9), which is made of a measured carbon composite and is partially covered by galvanically-deposited gold reflective layers on one side of the panel and by a nickel layer on the opposite side. In the middle, there is a bare composite material. These layers are used for determining the thermal transmissivity through the carbon material and also the reflectivity in the IR spectrum. The temperature throughput is measured as a temperature difference by a pair of PT1000 thermometers placed on the panel directly one above the other. There are three pairs of these thermometers, each for a different surface treatment.

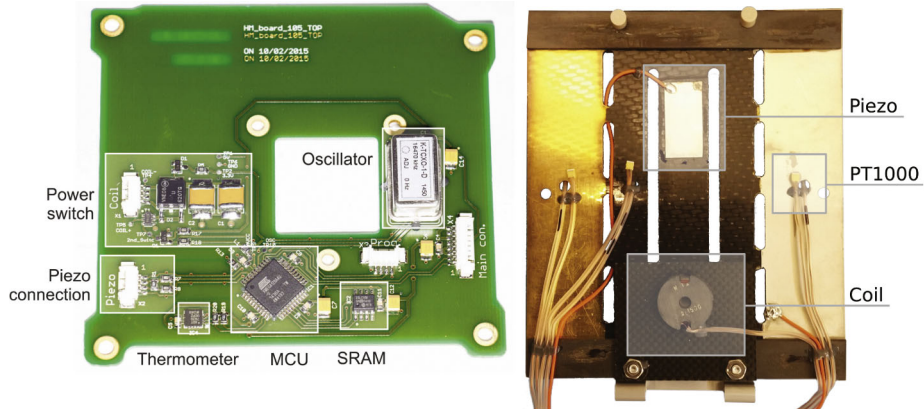


Fig. 9 Health monitoring panel (right) for measuring the mechanical properties of the carbon composite. The health monitoring board (left) manages the measurements of the mechanical properties (Urban et al. 2017)

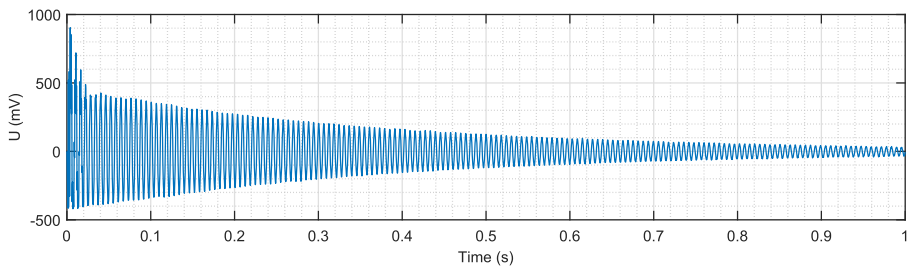
In the middle of the bare carbon material, a beam has been milled for measuring the mechanical properties. A permalloy target is placed on the free end. This target is attracted by the electromagnetic coil placed above it. The beam produces damped oscillations, which are measured by a piezo element located at the fixed end. All these parts are connected to the HM board which is on the right Fig. 9.

The sampled signal is processed onboard the satellite by the HM board's microcontroller. A fast Fourier transform (FFT) determines its eigenfrequencies and its oscillation attenuation. An important part of the signal processing electronics is the temperature-stabilized oscillator, which provides a stable frequency source. The data processing parameters can be changed by commanding the satellite from the ground station. For the volume of data, only three frequencies, attenuation, temperatures are sent to the Earth. The whole signal can be downloaded, but only on demand directly after measurements have been made. The full signal from the orbit is shown in Fig. 10a and its spectrum is shown in Fig. 10b. The measured first eigenfrequency of the beam is at 165 Hz. A task for us is to examine how this frequency will shift, and thus how the stiffness of the material will change.

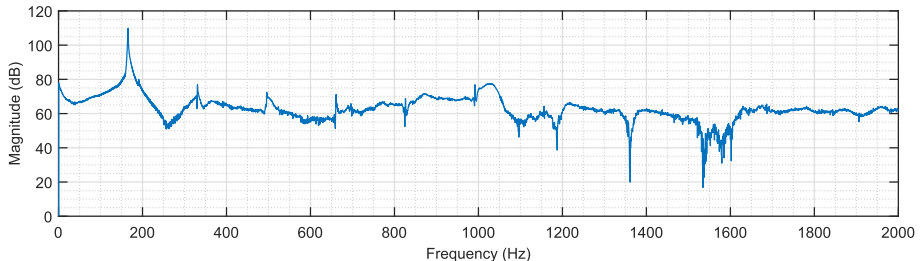
Until now (April 2018), the HM board has made more than 1500 usable measurements for future processing. The first results were published in Nentvich et al. (2018), and they showed the dependence of the first eigenfrequency in time. Figure 11a presents the frequency drift in dependence on the temperature of the composite in time (color series from earlier samples to more recent samples: blue, red, yellow and purple). The changes in the first eigenfrequency vary within a range of 2 Hz with a central peak at 165 Hz. Figure 11b shows is drawn the second eigenfrequency, which vary within a range of 23 Hz. From these two Figures, it is clear that the examined carbon fiber material is degrading because of the space environment, mainly due to radiation. The degradation rate is approximately 0.1 GPa per half of one year. In this case from 34.6 to 34.5 GPa.

3.4 Radiation Properties

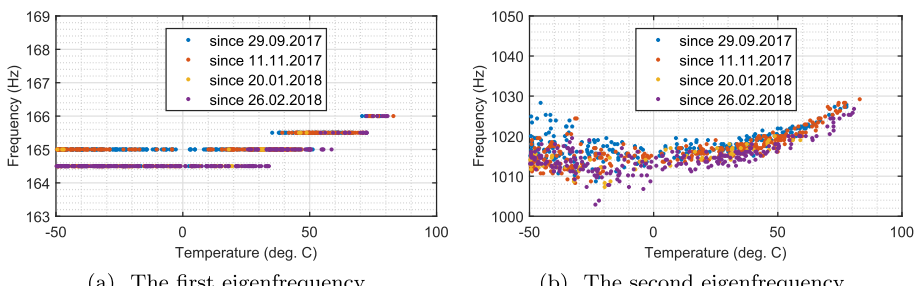
One of the main tasks on-board the satellite is to verify the radiation shielding properties of the tested carbon composite materials. Mathematical simulations were performed to estimate the real in-orbit radiation behavior. To determine the total radiation dose and the shielding effect of the composite, its properties are tested using comparative measurements



(a) The entire signal from the HM panel downloaded from orbit.



(b) The spectrum of the sensed signal (Fig. 10a) in the range to 2 kHz with dominant a peak at 165 Hz.

Fig. 10 Example of the sensed signal in orbit in shade at temperature -47°C **Fig. 11** Frequency changes of the eigenfrequency in dependence on the time from the beginning of the mission until April 2018

on three sensors, creating a radiation monitor on the XRB board and the Measure board (Urban et al. 2017). Each measuring channel consists of a sensor—an XRB PIN (p-type, i-intrinsic, n-type layer) diode, a sensitive amplifier of weak signal and an A/D transducer. The digitized signal is processed by fast CPLD, and is fed into the processor unit on the Measure board.

The silicon-based XRB diodes mounted on the XRB board can detect energies ranging from 5 keV to 100 keV. For higher energies, the X-Ray detection efficiency drops rapidly. Sensitivity at higher energies was improved by connecting a bias voltage at a level of 60 V. The detection efficiency decreases only slowly for particle detection. The amplifier was designed to detect a single events, taking into account the weakness of the useful signal. The signal from the detector is protected against cross-talk with the power system and against

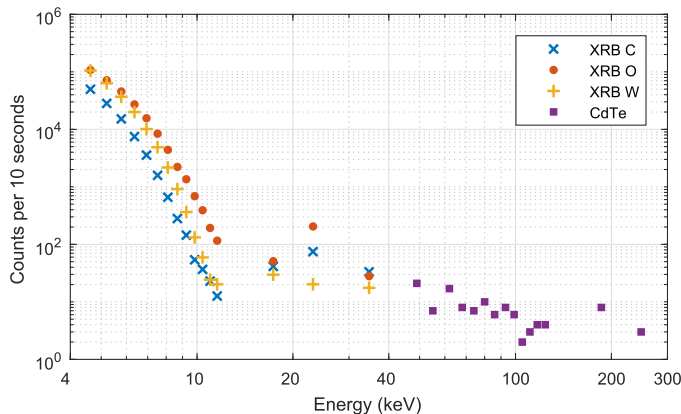


Fig. 12 The response of XRB sensors: Sum of the counts per 10 seconds above a threshold. The threshold was set to ≈ 4 keV. Differences in the sensitivity level of diodes and the noise edge at about 12 keV can be recognized

digital communication in the satellite shielded by conductive barriers, and individual parts were manually selected to minimize noise. The single event energy that is detected can be used for spectrum measurements for each diode.

The tests on the quality of the shielding itself are based on a comparison of the intensity of the signal from all three channels. The XRB board is shielded from behind and from the sides by a Tungsten sheet 1 mm thickness to avoid the influence of radiation from the body of the satellite, and of space radiation coming through the body. The front side with active diode surfaces has three different levels of shielding. The first diode is open to free space (XRB O), shielded only by a thin gold foil (for protection against light), the middle diode is protected by the composite (XRB C), and the last diode is protected by a sandwich with the examined composite enveloping a sheet of Tungsten 0.5 mm in thickness (XRB W). Three channels were cross-calibrated on the ground using an Americium X-Ray source. An additional channel on the Measure board is used with the CdTe detector placed inside the satellite to measure the higher energies.

An example of the counts measurements over a time period of 10 seconds at mean a temperature of 7 °C of the XRB diodes and the CdTe detector is presented in Fig. 12. This was performed with the threshold setting for the XRB diodes ranging from low energy (4 keV) to high energy (40 keV) during real-time contact of the satellite flying in the range of the ground station located in Pilsen (Czech Republic). The threshold sets the lowest energy over all counts are measured. Figure 12 shows the noise of the diodes around 12 keV and the hit counts above this boundary. Measurements over central Europe are planned twice a day to provide the long-time changes in the radiation shielding properties of the studied composite material. The diode and/or the properties of the electronics can change over time, and the ability to capture useful signals can drop. These changes will influence the noise edge as a rise in the main trend. Orbital results after 6 months of operation have revealed no degradation of the diodes signal so far.

The result of periodic measurements over the period of four months from November 2017 to February 2018 are presented. All measurements were made over central Europe at an altitude of about 500 km. An exposition time of 5 seconds was used for all measurements on all thresholds. The data are presented by descriptive statistics, using boxplots. The red line represents the median value, the blue box represents 50% of all the data, the whiskers

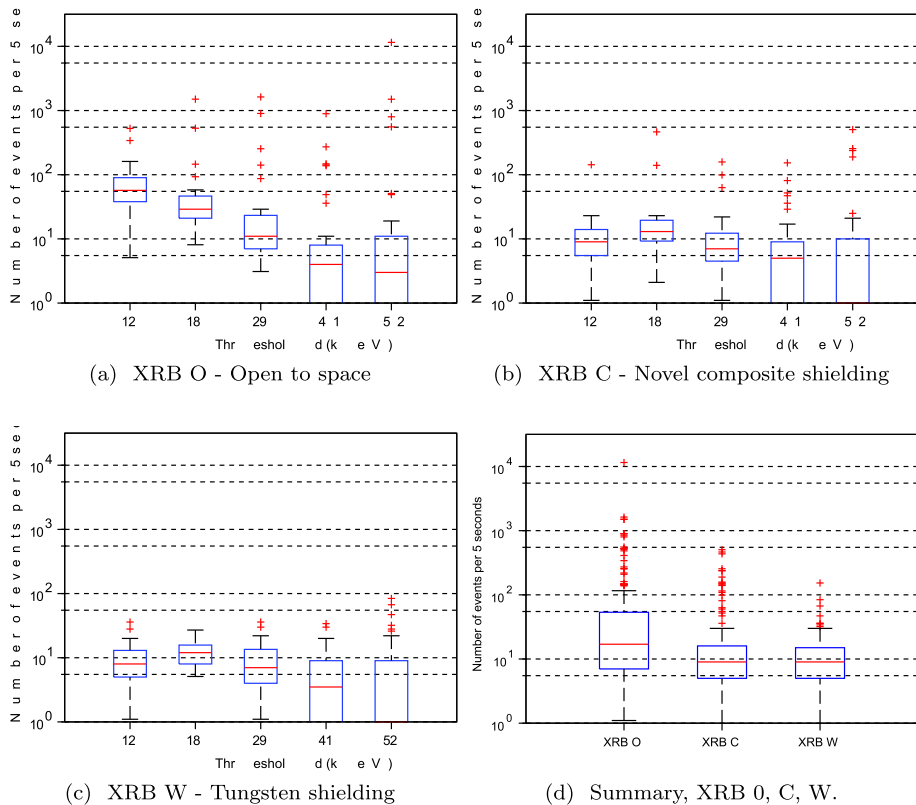
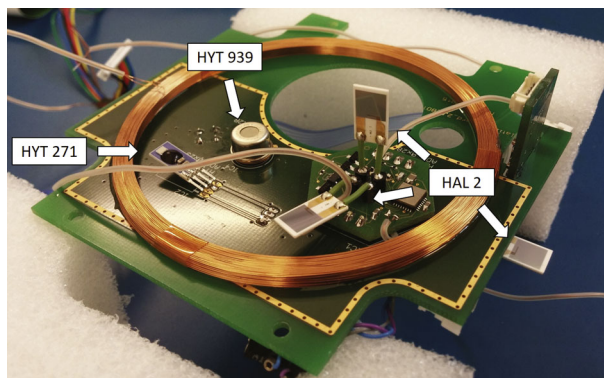


Fig. 13 XRB diodes measurement over central Europe twice per day over a period of four months. (a) XRB O is the diode open to space measurement, (b) XRB C refers to measurements under the novel composite shield, (c) XRB W refers to measurements under the composite and tungsten shield. (d) A summary of measurements taken twice per day over a period of four months over central Europe, 5 second exposition over 12 keV

represent 99.3% of all data, and the red crosses represent the measurement outliers in 0.7% of the data. The number of events per 5 seconds of exposition is presented in Fig. 13d. Events above the 12 keV threshold are presented. Over time the measured event count varies from 0 events up to 10^4 hits per 5 seconds. The number of outliers increases with the number of events (red crosses). These are probably caused by X-Ray flashes or by gamma-ray bursts. The shielding effectiveness can be estimated by comparing the total number of events. An XRB O diode open to space with no shielding has a median of 18 events per 5 seconds of exposition. The novel composite shielding has a median value of 9 events per five seconds. XRB W has a shield composed of the stack the tungsten and novel composite. The median value of XRB W is comparable with the XRB C signal. In addition, XRB W also provides shielding against hi-rate events a smaller number of outliers (red crosses). The stack of tungsten and the novel composite provides the most effective shielding.

The data are separated into groups for XRB O (Fig. 13a), XRB C (Fig. 13b), and XRB W (Fig. 13c), partitioned by the threshold energy. Energies over 30 keV have an uniform distribution, not the Gaussian distribution. The median or mean value does not provide a good description of this data group. For a threshold of 18 keV, the median of events for an open

Fig. 14 Volatiles board with three types of sensors (HYT 271, HYT 939 and HAL2) and a double magneto-torquer coil for the Z axis (Urban et al. 2018)



diode has as a value 29; for a diode under the composite, the value is 13; and for a diode under a tungsten and composite stack, the value is 12. For a threshold of 12 keV, the median of events for an open diode is 57; for a diode under the composite, the value is 9; and for a diode under tungsten and composite, the value is 8. By comparing these values, we can calculate a composite shielding effectiveness value of 84% for energies below 18 keV, and shielding effectiveness of 55% for energies below 29 keV. For energies above 29 keV, the mean shielding effectiveness is about 36%. For a composite and tungsten stack, we can calculate shielding effectiveness of 86% for energies below 18 keV, and shielding effectiveness of 58% for energies below 29 keV. For energies above 29 keV, the mean shielding effectiveness is about 36%. XRB W also provides shielding for burst events (smaller numbers of red crosses indicating outliers). The stack composition also serves for shielding the secondary radiation from the tungsten layer. We can observe no increase in low energy rates for XRB W over the XRB C data. The stack of tungsten and the novel composite provides the most effective shielding.

3.5 Volatiles

Verification of the properties of the new carbon fiber composite material (Daniel et al. 2016) includes not only the radiation resistance measurements (3.4) and the measurements of the mechanical properties (3.3), but also evaporation measurements of the water vapor and other gases from the material. It is important to make measurements of the residual humidity in space to validate the outgassing properties of the material. In the first days following the launch into orbit, there is evaporation effect the most significant. This indicates the existence of water vapor around and in the satellite. The evaporation can be very hazardous for the optics, the detector and other sensitive parts of the satellite. Condensation effects can occur in various locations on the satellite during thermal cycling (the temperature varies between -50°C and $+80^{\circ}\text{C}$ outside the satellite in case of VZLUSAT-1) (Urban et al. 2017). Moisture may damage the sensors or short-circuit the electronic boards (some types of experiments are using voltage between tens and one hundred volts). These experiments can be switched on only when evaporation is at the safety level. For this reason, special sensors are needed for measurements of trace amounts of gas in vacuum.

There are three types sensors of volatiles on board the VZLUSAT-1 satellite (see Fig. 14). From both sides of the Volatiles board there are two pairs of organic polymer sensors HYT 939 and HYT 271. These types of sensors provide temperature and relative humidity measurements via the I2C interface. The third kind sensors of volatiles are inorganic HAL2

Fig. 15 Thermal characteristic of the HAL2 sensor (placed inside the satellite) measured during measurements lasting several hours (orbits). Preliminary results provide 991 samples of measured data, out of which 144 samples are excluded

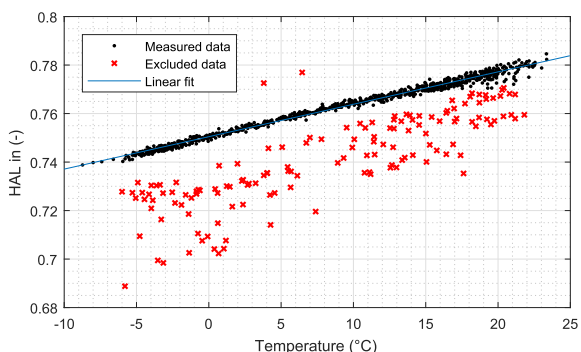
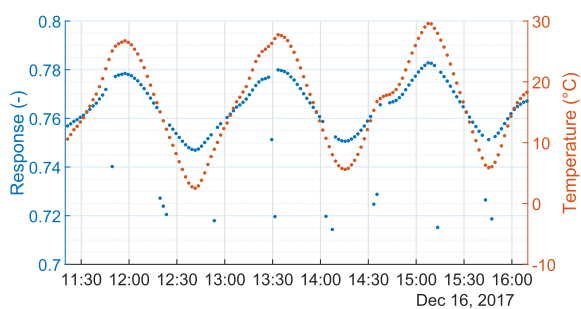


Fig. 16 The response of inorganic sensor HAL2 and its temperature over time (Urban et al. 2018)



sensors based on Aluminium oxide (Al_2O_3). The experimental readout is based on measurements of the charging/discharging time of the Al_2O_3 layer structure, and a comparison between it and a reference circuit. There are three samples of this kind of sensor. The first sample is located directly on the Volatiles board, and the second leads through to the radio board farther into the satellite. The last HAL2 sensor is placed outside VZLUSAT-1, with the active layer in the direction of flight. Since these sensors are not equipped with integrated temperature measurements, it was necessary to add platinum thermometers on their rear side.

Several measurements were made during the first days after launch. The data provide the first information about characteristics of the sensors and the level of evaporation from the satellite. The preliminary temperature characteristic of one of the HAL2 sensors was measured in space, and is shown in Fig. 15. Measurements were obtained during several orbits and thermal cycling. This characteristic corresponds to the measurements made on the ground before the start. An example of the time course of one of the measurements during thermal cycling is shown in Fig. 16. An analysis of this signal showed that cycling occurred with a period of about 94 minutes. This corresponds with the CubeSat orbit, i.e. with its movement on the day side and the night side of Earth. The temperature dependence can be well fitted by a linear function, seen in Fig. 17b. Malfunctions during readout and system restarts cause excluded data. Excluded data are labelled in Fig. 17b and are also shown in Fig. 16.

The very first processed data from the sensors are plotted in Fig. 17. The figure also shows the temperature dependence of both kinds of sensors. The polymeric sensor HYT (Fig. 17a) exhibits hysteresis (blue), but this property was not seen on the sensors of inorganic HAL (Fig. 17b). On the contrary, decreasing value of the response (measured values)

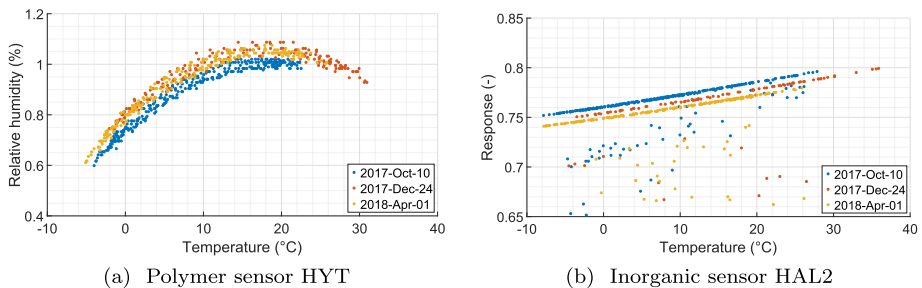


Fig. 17 The response of volatiles sensors in relation to their temperature over time (Urban et al. 2018)

from the sensors can be observed on these sensors. This behavior corresponds to a decreasing concentration of water molecules, according to ground experiments. It should be noted that polymer sensors are used at their operating threshold, unlike Al_2O_3 sensors, which are designed to measure trace moisture. Given these results and their mutual variations, it is necessary to eliminate the temperature dependence for a more accurate evaluation of the response of the sensor by further post-processing and deeper processing of differential values from the sensors in the context of the next measured satellite parameters.

Further measurements are scheduled at periodical intervals, and changes in the evaporation of water vapor from the body of the satellite can be estimated from the change in their response.

After three months of operation, we have successfully completed more than 14 sets of individual measurements by the Volatiles sensors. Each of them has more than 100 measured points at different temperatures and in different locations on the orbit. In total, we have already measured over 2000 points, from which we can further evaluate the decreasing concentration of the evaporation.

3.6 Experimental Solar Panels

The composite material for the radiation shield is proposed for use as a structural material for the satellite, and also as a base material for the solar panels. Solar panels commonly have a large surface area and small thickness. High mechanical stability is required together with low mass and volume. The experimental solar panels were developed on the basis of the radiation shielding material described in the sections above. There are two 1 U solar panels on the VZLUSAT-1 nanosatellite one is placed on the wall of the satellite, and the other can be deployed for extending the area and power sources. The Electronic Power System has worked satisfactorily from the first contact. The experimental and commercial solar panels show similar behavior. The batteries are charged continuously, and no high power consumption has been required.

3.7 Ground Station

The low altitude sun synchronous polar orbit limits the number and the duration of satellite passes within the range of the ground station (GS). One GS encounters approx. six satellite passes per day, each providing only a few minutes of effective data communication. Thus the amount of data transmitted between the satellite and the GS over a radio channel in an amateur UHF band is limited. The GS was designed for computer-assisted operations

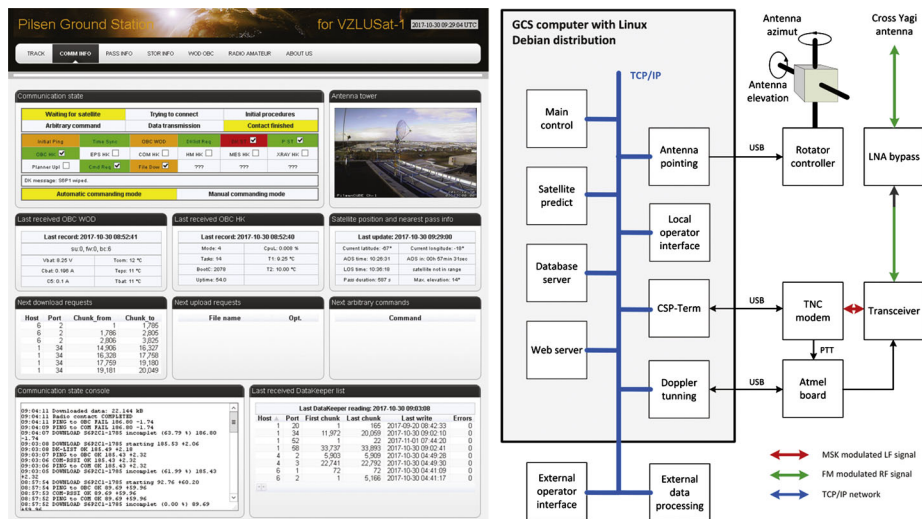


Fig. 18 Web interface for the ground station operators and a diagram of the ground station (Vertat et al. 2017)

at nights, during the weekends, and also for fully autonomous operations under operator supervision only.

The ground control station consists of hardware and software for processing information signals (commands, data) and control signals (transmit/receive, antennas targeting, Doppler shift tuning), interconnected as shown in Fig. 18. The main part of the GS consists of the antennas system with bi-axial AlfaSpid rotator, an ICOM IC-910h transceiver, a GomSpace TNC modem and a control computer with software. Based on the level of automatization, GS can be operated in manual, computer assisted or fully autonomous mode. The fully autonomous mode means that the entire GS is controlled by software based on pre-programmed logic, only under operator supervision (Vertat et al. 2017).

During early commissioning, manual mode was mainly used, because the radio communication with the satellite was not stable due to the spatial proximity of many satellites (31 satellites were released by the PSLV C38 rocket), the proximity of their communication frequencies and the proximity of their ground stations. This caused strong interferences, especially over Europe. In addition, some surveillance radar can also jam particular frequencies in the satellite receiver, as was examined in Busch et al. (2015). In the later phase of commissioning (after the radio link had stabilized) computer-assisted mode started to be widely used. Fully autonomous mode is commonly used for downloading large data sets during passes at night or during holidays, under GS remotely supervised by an operator. After the commissioning phase, we were able to reach the download capacity of approx. 200 kB per one day, on average, and all planned experiments were sufficiently satisfied in relation to data download requirements.

4 Conclusions

The VZLUSAT-1 satellite was successfully deployed into a circular polar orbit at an altitude of 505 km. The commissioning phase was successfully concluded. As of February 2018, the

satellite exceeded 240 days of successful operation following its deployment in low-Earth orbit. During commissioning, several difficulties regarding remote commanding, on-board data handling and the ADCS system were encountered. Some of the payloads also provided the team with unforeseen challenges. However, most of the difficulties were resolved by on-the-flight configuration and by direct commanding via the uplink. With the exception of the FIPEX instrument, the payloads are currently working properly and are collecting data. Measurements are being conducted regularly, with data being successfully downloaded by the ground segment. The polar orbit covers the polar horns and also the South Atlantic Anomaly, so the satellite is periodically exposed to high levels of in-orbit ionizing radiation. Due to the radiation, the expected lifetime is estimated to be one year. Up to February 2018, technological and scientific data were produced and retrieved regularly and the data have been presented. The measurements are also continuing to fulfill the long-term objectives of the mission.

Acknowledgements The work presented in this paper was performed as a cooperative effort carried out by the following companies: Czech Aerospace Research Centre a.s., TTS, s.r.o.—Thin-film Technological Services, s.r.o., Rigaku Innovative Technologies Europe s.r.o., 5M s.r.o., HVM PLASMA spol. s.r.o., IST s.r.o., and also the Czech Technical University in Prague, the University of West Bohemia, and the Charles University in Prague. The project has been supported by Czech Republic grants TA03011329, TA04011295, GA13-33324S and GJ18-10088Y.

Publisher's Note Springer Nature remains neutral with regard to jurisdictional claims in published maps and institutional affiliations.

References

- J.R.P. Angel, Lobster eyes as X-ray telescopes. *Astrophys. J.* **233**, 364 (1979)
- T. Baca, M. Platkevici, J. Jakubek, A. Inneman, V. Stehlíkova, M. Urban, O. Nentvich, M. Blazek, R. McEntaffer, V. Daniel, Miniaturized X-ray telescope for VZLUSAT-1 nanosatellite with Timepix detector. *J. Instrum.* **11**(10), C10,007–C10,007 (2016)
- S. Busch, P. Bangert, S. Dombrovski, K. Schilling, UWE-3, in-orbit performance and lessons learned of a modular and flexible satellite bus for future pico-satellite formations. *Acta Astronaut.* **117**, 73–89 (2015)
- V. Dániel, L. Pína, A. Inneman, V. Zadražil, T. Báča, M. Platkevič, V. Stehlíková, O. Nentvich, M. Urban, Terrestrial gamma-ray flashes monitor demonstrator on CubeSat, in *CubeSats and NanoSats for Remote Sensing*, vol. 9978 (SPIE, Bellingham, 2016), p. 99780D
- V. Daniel, M. Urban, O. Nentvich, V. Stehlíkova, VZLUSAT-1: verification of new materials and technologies for space, in *CubeSats and NanoSats for Remote Sensing*, vol. 9978 (SPIE, Bellingham, 2016), p. 99780N
- V. Dániel, A. Inneman, L. Pína, V. Zadražil, T. Báča, V. Stehlíková, O. Nentvich, M. Urban, V. Maršáková, R. McEntaffer, J. Tutt, T. Schulz, X-ray Lobster Eye all-sky monitor for rocket experiment, in *EUV and X-Ray Optics: Synergy Between Laboratory and Space V*, vol. 10235 (SPIE, Bellingham, 2017), p. 1023503
- C. Granja, S. Polansky, Z. Vykydal, S. Pospisil, A. Owens, Z. Kozacek, K. Mellab, M. Simcak, The SATRAM Timepix spacecraft payload in open space on board the Proba-V satellite for wide range radiation monitoring in LEO orbit. *Planet. Space Sci.* **125**, 114–129 (2016)
- P. Hana, A. Inneman, V. Daniel, L. Sieger, M. Petru, Mechanical properties of carbon fiber composites for applications in space, in *Optics and Measurement Conference*, ed. by J. Kováčičinová, T. Vít (2015), p. 94420A
- R. Hudec, Astrophysical payloads for picosatellites. *Contrib. Astron. Obs. Skaln. Pleso* **47**(2), 143–150 (2017)
- X. Llopard, R. Ballabriga, M. Campbell, L. Tlustos, W. Wong, Timepix, a 65k programmable pixel readout chip for arrival time, energy and/or photon counting measurements. *Nucl. Instrum. Methods Phys. Res., Sect. A, Accel. Spectrom. Detect. Assoc. Equip.* **581**(Spec. Iss. 1–2), 485–494 (2007)
- O. Nentvich, M. Urban, V. Stehlíkova, L. Sieger, A. Inneman, VZLUSAT-1: health monitoring system, preliminary results. *Astron. Nachr.* **339**(5), 397–402 (2018)

- L. Pína, R. Hudec, A. Inneman, D. Cerna, J. Jakubek, L. Sieger, V. Dániel, W. Cash, L. Mikulickova, R. Pavlica, E. Belas, J. Polak, X-ray monitoring for astrophysical applications on Cubesat, in *EUV and X-Ray Optics: Synergy Between Laboratory and Space IV*, vol. 9510 (SPIE, Bellingham, 2015), p. 951005
- L. Pína, R. Hudec, A.J. Inneman, T. Baca, M. Blazek, M. Platkevicius, L. Sieger, D. Doubravova, R.L. McEntaffer, T.B. Schultz, V. Dániel, Development and tests of X-Ray multifoil optical system for 1D imaging (Conference Presentation), in *Advances in Laboratory-Based X-Ray Sources, Optics, and Applications V*, vol. 9964 (SPIE, Bellingham, 2016), p. 99640B
- W. Schmidt, A proposed X-ray focusing device with wide field of view for use in X-ray astronomy. *Nucl. Instrum. Methods* **127**(2), 285–292 (1975)
- V. Stehlíkova, M. Urban, O. Nentvich, V. Daniel, L. Sieger, J. Tutt, Hard X-ray Vela supernova observation on rocket experiment WRX-R. *Contrib. Astron. Obs. Skaln. Pleso* **47**(2), 165–169 (2017)
- D. Turecek, L. Pinsky, J. Jakubek, Z. Vykydal, N. Stoffle, S. Pospisil, Small Dosimeter based on Timepix device for International Space Station. *J. Instrum.* **6**(12), C12,037–C12,037 (2011)
- M. Urban, O. Nentvich, V. Stehlíkova, T. Baca, V. Daniel, R. Hudec, VZLUSAT-1: nanosatellite with miniature lobster eye X-ray telescope and qualification of the radiation shielding composite for space application. *Acta Astronaut.* **140**, 96–104 (2017)
- M. Urban, O. Nentvich, V. Stehlíkova, L. Sieger, L. Mikulickova, Outgassing monitor on VZLUSAT-1: preliminary results. *Astron. Nachr.* **339**(5), 367–370 (2018)
- I. Vertat, R. Linhart, L. Dudacek, V. Daniel, P. Svoboda, Autonomous and semi-autonomous radio commanding of VZLUSAT-1 nanosatellite from ground control station in Pilsen, in *2017 International Conference on Applied Electronics (AE)* (IEEE Press, New York, 2017), pp. 1–6
- Z. Vykydal, J. Jakubek, USB lite—miniaturized readout interface for Medipix2 detector. *Nucl. Instrum. Methods Phys. Res., Sect. A, Accel. Spectrom. Detect. Assoc. Equip.* **633**, S48–S49 (2011)